Int. J. Heat Mass Transfer. Vol. 36, No. 13, pp. 3383–3392, 1993
Printed in Great Britain

0017–9310/93 $6.00 + 0.00

Flow structure and turbulent transport of a supercritical pressure fluid in a vertical heated tube under the conditions of mixed convection. Experimental data

V. A. KURGANOV and A. G. KAPTILNYI
Institute for High Temperatures, Russian Academy of Sciences, Moscow, 127412, Russia

(*Received* 14 *August* 1991)

Abstract—Experimental data on the velocity and temperature fields of a heated turbulent supercritical-pressure carbon dioxide flow in a 22.7 mm dia. vertical tube under the conditions of mixed convection are obtained. A comparative analysis of the results of measurements for buoyancy assisted and opposed upward and downward flows has allowed a conclusion that a relative deterioration in heat transfer in the case of an upward flow with the development of the inlet wall temperature peaks is attributable to the rearrangement of velocity fields and shear stresses in the course of which a fluid layer with reduced turbulence generation appears. Based on the results of measurements of velocity and temperature fields, heat transfer and hydraulic drag, the profiles of shear stresses and heat fluxes as well as the eddy diffusivities and turbulent Prandtl numbers have been calculated which are compared with some turbulent transfer models applied for calculating heat transfer in the supercritical region.

1. INTRODUCTION

MIXED convection is of frequent occurrence in tubes in the processes of heating supercritical-pressure fluids that have low viscosities and high thermal expansion coefficient which passes through a maximum in the vicinity of t_m. Moreover, a substantial dependence of the level and behaviour of heat transfer on flow direction with respect to the gravity is observed [1, 2]. In vertical uniformly heated (q_w = const.) tubes, which will be considered in what follows, the heat transfer coefficient for an upward flow can vary appreciably along the tube length resulting in the so-called inlet wall temperature peaks. These peaks may be hazardous for the tube, especially when they develop under substantially non-isothermal conditions, i.e. at great temperature drops between the wall and the flow (and, correspondingly, at great values of ρ_b/ρ_w).

In the case of the supercritical water or CO_2 flow in a tube having the diameter of about 20 mm, such a situation is typical of the region of 'mean' mass velocities of the heat transfer agent, $m_b \approx 600$–1500 kg m^{-2} s^{-1}. For a downward flow in the indicated conditions the inlet peaks of t_w are not observed and the heat transfer rate is higher and more uniform. At the present time, the mixed convection heat transfer in the near-critical region can be calculated only with an appreciable and almost unpredictable error, especially for an upward flow. This refers to both the calculations from the empirical formulae available in literature and numerical solutions of a system of differential equations for the process. Thus, in refs. [3–5], in which the buoyancy effect was taken into account only at the level of an averaged flow, the results of calculations are at variance with the experimental data and predict an increase in the heat transfer rate for an upward flow and its decrease for a downward flow. In refs. [6, 7] the models of turbulent transfer have been developed which take into account the direct effect of buoyancy. In a number of cases these models allow one to obtain a satisfactory agreement with the experimental heat transfer data [8, 9]. Unfortunately, the development of such models for the near-critical region is impeded by the paucity of reliable experimental data on hydraulic drag and internal flow structure. The previous relevant publications [10–14] have a number of methodological drawbacks which have already been pointed out earlier [15, 16]. Therefore, the problem of obtaining reliable experimental data on the structure of turbulent flows in the near-critical region still remains particularly urgent.

The present paper suggests experimental data on the structure, heat transfer and hydraulic drag of supercritical-pressure carbon dioxide, CO_2, heated in a vertical tube and flowing upwards or downwards with the mass velocity $m_b = 800$ and 1200 kg m^{-2} s^{-1}, respectively. The tube diameter is $d = 22.7$ mm, the pressure of CO_2 is $P = 9.0$ MPa; the air admixture in CO_2 is of about 0.5 mole %. The experimental technique is described in detail elsewhere [16, 17]. It needs only be repeated that measurements were carried out within the range $0 \leqslant R \leqslant 0.995$ with a small Pitot tube and microthermocouples; for each mode of heat transfer 6–9 pairs of velocity and temperature profiles were measured along the tube length starting from $x/d = 2.5$ and thereafter with a step of $15d$. Simultaneously, the distribution of static pressures

NOMENCLATURE

a thermal diffusivity
$B(Pr)$ constant in logarithmic enthalpy profile
c_p specific heat at constant pressure
d tube diameter, $2r_0$
g gravitational acceleration
G projection of acceleration of body forces on fluid flow direction (axis x), $-\left[\pm g+\left(u\frac{\partial u}{\partial x}+v\frac{\partial u}{\partial r}\right)\right]$
Gr_ρ Grashof number, $\frac{gd^3}{\nu_b^2}\left(1-\frac{\rho_w}{\rho_b}\right)$
h enthalpy
h^+ dimensionless enthalpy, $(h_w-h)\rho v_*/q_w$
K parameter of fluid acceleration, $K_u \pm K_g$ (plus sign for upward flow, minus sign for downward flow)
K_{HJ} parameter of the Hall and Jackson buoyancy effect [2, 18]
K_u parameter of thermal acceleration [15]
K_g parameter of the effect of Archimedes forces, $Gr_\rho/(\xi Re_b^2)$
l mixing path length
m mass velocity, ρu
Nu Nusselt number
P pressure
Pr Prandtl number
$\overline{Pr}$ mean Prandtl number, $Pr_b[(h_w-h_b)/(t_w-t_b)]/c_{pb}$
Pr_t turbulent Prandtl number, $\varepsilon_\tau/\varepsilon_q$
q heat flux density in radial direction
r radius
r_0 tube radius, $d/2$
R dimensionless radius, r/r_0
Re_b Reynolds number, $m_b d/\mu_b$
Ri gradient Richardson number, $\frac{G\beta\,\partial h/\partial r}{c_p\,\partial u/\partial r|\partial u/\partial r|}$
St Stanton number, $q_w/[m_b(h_w-h_b)]$
t temperature
u streamwise velocity component
u^+ dimensionless velocity, u/v_*
v radial velocity component
v_* dynamic velocity, $\sqrt{(\tau_w/\rho)}$
x longitudinal coordinate reckoned from the start of heating
y distance from wall along radius
y^+ universal coordinate, yv_*/ν
Y dimensionless distance from wall, $y/r_0 = 1-R$
Z_τ relative eddy diffusivity of momentum, $\varepsilon_\tau/\varepsilon_{\tau R}$
Z_q relative eddy diffusivity of heat, $\varepsilon_q/\varepsilon_{\tau R}$.

Greek symbols

β coefficient of thermal expansion
ε_τ eddy diffusivity of momentum (1)
ε_q eddy diffusivity of heat (1)
λ thermal conductivity
μ dynamic viscosity
ν kinematic viscosity, μ/ρ
ξ coefficient of friction resistance
ξ_u coefficient of inertial resistance [15]
ρ density
τ shear stress.

Subscripts

b bulk values; at $h = h_b$
in at tube inlet
lim limiting value in normal heat transfer regimes
m at heat capacity maximum point at given pressure
max maximum value; at velocity maximum point
N in normal heat transfer regime
R according to Reichardt's model
stab under stabilized heat transfer conditions
t turbulent characteristics
w conditions on wall
0 at constant physical properties; when $Ri \to 0$.

along the tube was measured. In the regimes considered, the balance of profiles on mass flow rate, and also on heat when $x/d \geqslant 17.5$, converged with an error not exceeding $\pm 4\%$. Based on the results of thermal, hydraulic and probe measurements and using a system of integral continuity, motion and energy equations, the profiles of τ/τ_w and q/q_w were calculated, as well as the eddy diffusivities of momentum and heat:

$$\frac{\varepsilon_\tau}{\nu}=\frac{\tau}{\mu\,\partial u/\partial y}-1;\quad \frac{\varepsilon_q}{a}=-\frac{c_p q}{\lambda\,\partial h/\partial y}-1. \qquad (1)$$

The experimental data obtained were compared

between themselves, with the classical ideas on the structure of turbulent flows and with some turbulent transfer models used in calculations of heat transfer in the supercritical region.

2. HEAT TRANSFER AND FRICTION

The heat transfer regimes which will be considered in the paper are illustrated in Fig. 1. Among these, there are regimes with the 'inlet' wall temperature peaks of different intensity (Fig. 1(a)) and regimes with monotonous heat transfer distribution along the tube length (Fig. 1(b)) which can be regarded as being normal heat transfer modes [1]. However, already in these regimes a certain difference in the upward and downward flow heat transfer appears which allows one to speak about the start of the effect of buoyancy. In Fig. 1(c) the local Stanton numbers are compared with the normal heat transfer relation [15]:

$$St_N = \frac{\xi_N/8}{1+900/Re_b+12.7\sqrt{(\xi_N/8)}(\overline{Pr}^{2/3}-1)} \quad (2)$$

where

$$\xi_N/\xi_{ob} = (\rho_w/\rho_b)^{0.4} \quad (3)$$

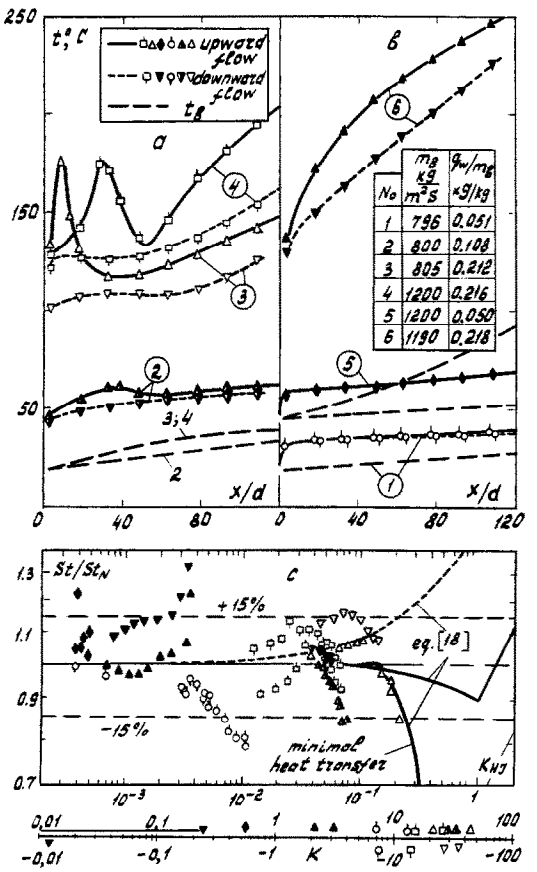

FIG. 1. Heat transfer regimes being discussed; wall and fluid temperature (a, b), heat transfer and acceleration parameter (c).

is the scaling law of friction for the pseudophase transition region and also with the empirical relation obtained in ref. [18] for mixed-convective heat transfer to a supercritical-pressure water. Among other formulae, this relation gave the most acceptable results when compared with the entire set of experimental data obtained by the present authors for heat transfer to CO_2 within the range $m_b = 50$–$800\ kg\ m^{-2}\ s^{-1}$ [17]. The replacement of the ratio Nu/Nu_N by St/St_N in this relation is of no importance.

The data of Fig. 1(c) show that the regimes studied are located at the edge of the region with a strong effect of buoyancy on heat transfer. At the bottom of Fig. 1(c), a scale is given on which the values of the acceleration parameter are indicated [15]:

$$K = K_u \pm K_g = \xi_u/\xi \pm Gr_\rho/(\xi Re_b^2) \quad (4)$$

(the plus sign refers to the upward, and the minus sign to the downward, flow). When $K_u \gg K_g$, i.e. if the effect of buoyancy was weak, the parameter K was successfully used [15, 19] for analyzing and correlating experimental data on deteriorated heat transfer. In this case, when values of Re are rather higher, $Re > 5 \times 10^4$, the region of normal heat transfer, equations (2), is determined by a simple condition

$$K \leqslant 1\text{–}1.3 \quad (5)$$

to which there correspond the asymptotic distributions of shear stresses at the wall:

$$(\tau/\tau_w)_{R\to 1} \cong R - 2KY \geqslant (\tau/\tau_w)_{lim} = 1 - 3Y. \quad (6)$$

When $K_g \geqslant K_u$, there is no simple relationship between the wall profile τ/τ_w and parameter K. Nevertheless, in this case too, it is convenient to use this parameter as a measure of the mutual relationship between the Archimedes, inertia forces and friction forces generated by the wall. In particular, all downward flow heat transfer regimes (Fig. 1), which satisfy condition (5) with some safety margin, have all the symptoms of normal heat transfer. The intrinsic (when $K_g \gg K_u$) effect of buoyancy in an upward flow allowing one to speak about the deterioration of heat transfer is observed only when $K \approx K_g \geqslant 7$ (regimes Nos. 1–4). If other experimental data [17], which are not considered here, are taken into account, then the start of the negative effect of buoyancy on heat transfer can be determined by the condition $K_g > 3$. These figures are close to the theoretical estimate $K_{glim} = 5$ obtained in ref. [20].

Experimental data on hydraulic and friction drag obtained in the works of the present authors for a large-diameter tube [21] allow a conclusion that under the conditions considered, with a substantial effect of buoyancy, there are no appreciable changes in the Boussinesq coefficient, i.e. the flow acceleration is well described by a one-dimensional model, whereas the friction drag obeys law (3) on the average. However, because of the relatively small value of the friction drag, the experimental values of ξ were obtained with a great error and their deviations from relation (3)

attained 25–40% at separate points. This accuracy is insufficient for analyzing the turbulent transport parameters. Therefore, in the case of appreciable deviations of experimental data of ξ from ξ_N, the variant processing of the results of probe measurements was carried out. This allowed one to evaluate the effect of the error in the determination of ξ on the sought-after parameters of the averaged flow and to select those values of ξ which would ensure the mutual agreement of the entire packet of test data and the consistency with the requirements of the limiting transition to the classical concepts about the structure of flow. The analysis has shown that the indicated consensus is attainable when the values of ξ used for processing test data fit relation (3) with a deviation within $\pm 5\%$ for an upward flow and within $0+$ (5–10%) for a downward flow. We shall come back to this problem in Section 4. Hereafter, if and when necessary, the indicated correction will be introduced into the test data presented in the figures with a special reference in the most important cases.

3. VELOCITY AND ENTHALPY PROFILES

A typical character of velocity profiles in the considered modes of heat transfer is shown in Fig. 2. In this and all the other figures, the data that refer to different heat transfer regimes are labelled by the same points as in Fig. 1. In the case of an upward flow (Figs. 2(a) and (b)) in regimes Nos. 1, 5 and 6 the profiles of u/u_b over the entire tube length retain a convex shape; however, as the parameter K grows, they become increasingly flatter in the central part and fuller near the wall. This deformation already occurs within the thermal entrance region whereas with $x/d > 30$ the changes in the profile of u/u_b are accumulated rather slowly.

With regimes Nos. 2–4 in an upward flow the parameter K is rather high—of the order of 30–50; an intensive velocity profile deformation takes place which in the approach to section $x/d = 32.5$ terminates in transition to an M-like form with the maximum not far from the wall and minimum on the tube axis. As shown in ref. [3], it is this very form of velocity which is capable of ensuring dynamic equilibrium between the Archimedes forces and shear stresses in the flow. Comparing the data of Figs. 1 and 2 shows that the formation of the inlet wall temperature peak coincides with the stage of transition from a very flattened to an M-like velocity profile. A similar conclusion can also be drawn regarding the profile obtained in ref. [13]. The velocity maximum has the greatest peak at the end of the heat transfer deterioration region, whereas downstream a gradual smearing of this maximum takes place. This is due to both the change in the thermodynamic state of the heated liquid, which leads to the general decrease in the Archimedes forces, and a high level (which will be shown below) of turbulent transport in the trough of the M-like profile.

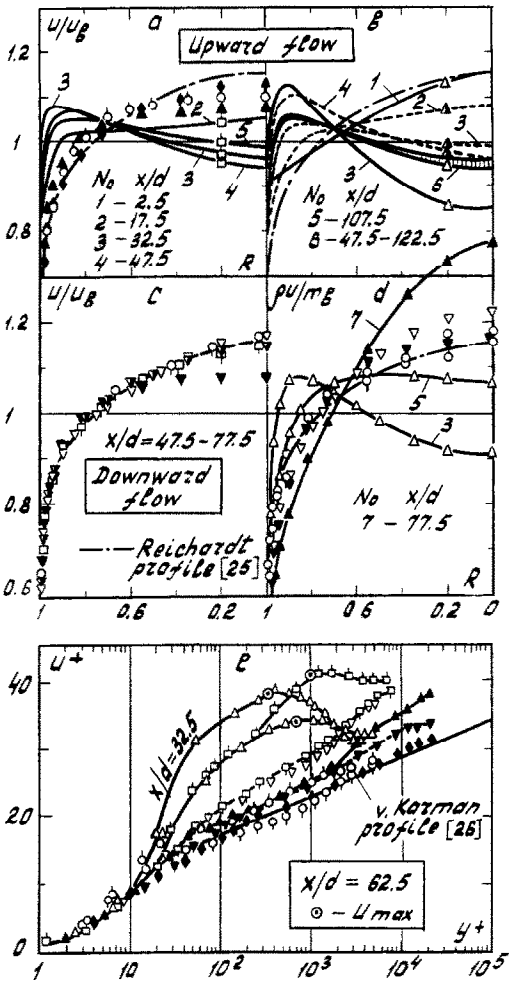

FIG. 2. Velocity profiles (a, b, c, e) and mass velocity profile (d).

In all the regimes with a downward flow, the shape of the u/u_b profile is retained which is usual for a turbulent flow, but with a certain trend toward flattening at the tube centre and filling in the outer region of the boundary layer (Fig. 2(c)). It should be noted here that with downward flow in the region with $R \leqslant 0.8$, slow fluctuations in the Pitot tube readings were observed which were not amenable to precise averaging. The construction of the measured velocity profiles has revealed that when $R < 0.8$ many profiles have a wavy form as though there was a system of almost immovable vortical rings in the tube. These observations may be indicative of the development of specific large-scale structures in downward flows. When analyzing the test data the waves on the velocity profiles were attributed to measurement errors and were smoothed-out. Figure 2(c) presents the smoothed-out profiles of u/u_b; the deviations of the test points from these curves may constitute ± 2–3%. The mass velocity profiles at a distance from the entrance are shown in Fig. 2(d). It is seen that in the

case of an upward flow with considerable effect of Archimedes forces the profiles of $\rho u/m_b$ also acquire an M-like shape; here the mass velocities in the wall region grow, being conducive to heat transfer intensification. Conversely, the more extended profile of ρu in regime No. 6 points toward a relative attenuation of heat transfer in the flow core. The typical form of velocity profiles in the wall law coordinates is shown in Fig. 2(e). The density and viscosity values for these variables were determined at the local enthalpy of the fluid. The points for regimes Nos. 4 and 6 were plotted at the corrected values of ξ. The points for $R > 0.995$ ($y^+ < 30$–100) have been obtained by matching the $u(R)$ curves in the zone of measurement with the curves in the laminar sublayer ($y^+ \leqslant 5$) calculated from the known values of t_w, q_w, and τ_w. It is seen that in the regimes with a relatively weak effect of buoyancy, a usual boundary layer structure with a logarithmic velocity profile section persists near the wall. Almost the same structure is also preserved in regimes Nos. 2–4 with a downward flow (the departure of the curves from the von Karman profile line is partially due to an appreciable change in the viscosity: $\mu_b/\mu_w \cong 2.3$). On the other hand, with an upward flow in these regimes the velocity profiles deviate considerably upward from the standard profile thus indicating a relative attenuation in momentum transfer over the stretch of the profile located between the buffer region and the velocity maximum. As will be shown below, it is just over this stretch that shear stresses decrease rapidly and pass through the zero value.

Figure 3 presents a typical form of the enthalpy fields and profiles in the considered regimes of heat transfer. From Fig. 3(a) it is seen that the input wall temperature peak is conditioned by the fluctuations of the thermal resistance of the thin wall layer; these perturbations have almost no influence on the flow core heating ($R < 0.95$). Beyond the peak region of t_w for an upward flow and outside the initial section ($x/d > 30$) for a downward flow, the heating of the flow approaches the uniform one

$$\partial h/\partial x \approx \partial h_b/\partial x. \tag{7}$$

In this case, when $\rho v \approx 0$, the distribution of heat fluxes is described by the relation [22]:

$$(q/q_w)_{stab} = \frac{2}{R}\int_0^R \frac{\rho u}{m_b} R\,dR. \tag{8}$$

The enthalpy profiles in the wall law coordinates are shown in Fig. 3(b) in comparison with the logarithmic profile at constant properties [23]:

$$h^+ = 2.12 \ln y^+ + B(Pr). \tag{9}$$

The determination of the constant $B(Pr)$ was made at $Pr = \overline{Pr}$ (for light points $\overline{Pr} \approx 1.7$ and $B \approx 11$; for dark points, 0.9 and 5). In Fig. 4, the comparison between the distributions of the enthalpy resistance in the flow for an upward and downward flow is given.

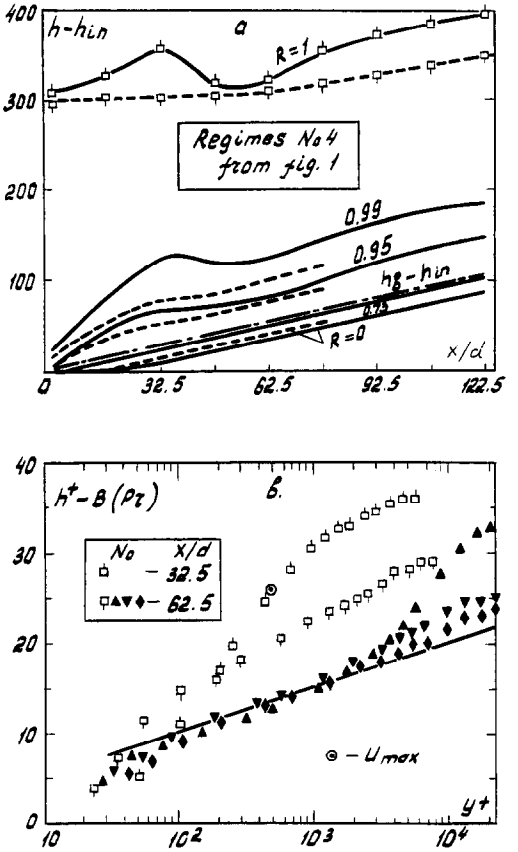

FIG. 3. Enthalpy field (a) and enthalpy profiles in the wall law coordinates (b).

Since

$$1/St = \int_0^1 u^+ h^+ \,dR^2, \tag{10}$$

the curves of Fig. 4 clearly show what flow regions are responsible for the observed differences in heat transfer. In regime No. 6 this is the central half of the

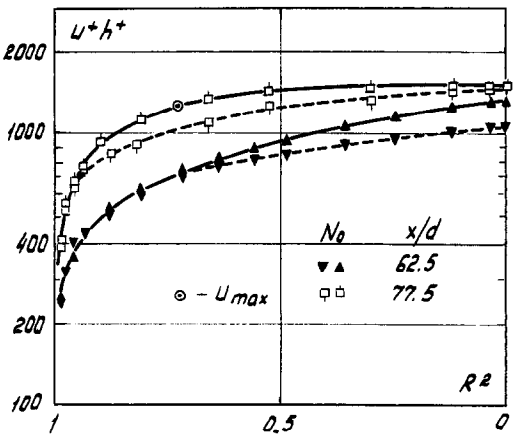

FIG. 4. Distribution of enthalpy resistance over the flow section.

flow; whereas in regime No. 4 and in similar regimes Nos. 2 and 3 this is the wall region which precedes the velocity maximum of the M-like profile. It is in these regions that the splitting of the u^+ and h^+ profiles also is observed in Figs. 2(e) and 3(b).

The τ/τ_w profiles in Fig. 5(a) show that the indicated regions of deteriorated heat transfer correlate with the location of the understated (near zero) shear stresses and transverse velocity gradients, i.e. with the regions of lowered turbulent energy generation at the expense of an averaged flow. In the considered cases of large Reynolds numbers these regions are located as a rule outside the viscous and buffer zones of the boundary layer and exert a weak effect on their thermal resistance.

Note that in regimes Nos. 1 and 6 with an upward flow, the distribution of τ/τ_w near the wall is located already somewhat below that of $(\tau/\tau_w)_{lim}$ obtained from equation (6), but the difference is still not so appreciable and the heat transfer is close to the normal one, equation (2). (When considering in Fig. 1(b) the points for regime No. 1, it is necessary to take into account that far from the entrance $t_w \approx t_m$; therefore, the accuracy with which the enthalpy differences and Stanton numbers are determined is not so precise here as in other regimes.) Thus, relation (6) can be used for controlling the 'normal value' of heat transferred. Hall and Jackson [2] assumed that the negative effect of buoyancy and acceleration on heat transfer would become noticeable if $\tau/\tau_w < 0.9$ at $y^+ = 30$. When thermal acceleration prevails ($K_u > K_q$), this condition cannot be true, and the deterioration of heat transfer develop when $(\tau/\tau_w)_{30}$ is closer to unity than to 0.9. In regimes Nos. 1 and 6, $(\tau/\tau_w)_{30} = 0.95$–$0.97$; but in all the regimes with the input wall temperature peak $(\tau/\tau_w)_{30} < 0.9$. Thus, in the regimes with the prevailing effect of Archimedes forces the criterion suggested in ref. [2] is confirmed by the results of the present measurements.

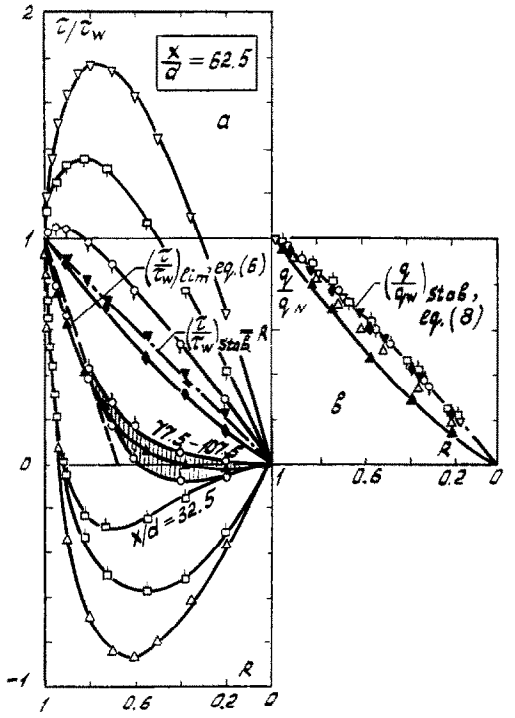

FIG. 5. Profiles of shear stresses (a) and of radial heat fluxes (b).

Figure 5(b) shows that the profiles of q/q_w far from the entrance adhere well to relation (8). (In different regimes the curves $(q/q_w)_{slab}$ differ somewhat from one another. In Fig. 5(b) the 'medium' curve has been drawn; the deviations of other curves from this one are of minor importance as compared with the scatter of test points.)

An exception is the q/q_w profile in regime No. 6 with an upward flow. It indicates a delay in heating the central portion of the flow as compared with the entire flow and the overheating of the wall layers which compensates for this delay. This pattern is typical of the cases of heat transfer deterioration at moderate values of the parameter K, when deformations of the flow develop rather slowly along the tube length. Similar cases, which are especially characteristic for high mass flow velocities, were considered in refs. [16, 24].

4. TURBULENT TRANSPORT

Experimental data on turbulent transport are presented in Figs. 6–8. According to equation (1), the values of ε_τ and ε_q are related to the values of $\varepsilon_{\tau R}$ calculated by Reichardt's equation [25]:

$$\varepsilon_{\tau R}/\nu = 0.4\left(y^+ - 11\tanh\frac{y^+}{11}\right), \quad \text{when} \quad y^+ \leqslant 50$$

$$\varepsilon_{\tau R}/\nu = 0.4y^+\frac{(0.5+R^2)(1+R)}{3}, \quad \text{when} \quad y^+ > 50. \tag{11}$$

The results of calculations show [8, 9, 22], that the Reichardt model with the local properties at $Pr_t \simeq 0.9$–1 allows one to describe rather well experimental data on normal heat transfer to various fluids with variable properties. This provides a reason to adopt the values given by equations (11) as 'normal values' of eddy diffusivity which would have occurred in the absence of the effect of buoyancy and thermal acceleration.

In Figs. 6–8 the local values of ε_τ and ε_q are presented for $y^+ > 100$ and $R > 0.2$ when the velocity and enthalpy deviations with respect to the radius can be determined with an acceptable accuracy. In close vicinity to the wall, a numerical solution of equations (1) at the known values of q_w, t_w, τ_w, τ/τ_w, and q/q_w was made. The values of ε_τ and ε_q were prescribed in the form

$$\varepsilon_\tau = \bar{Z}_\tau\varepsilon_{\tau R}; \quad \varepsilon_q = \bar{Z}_q\varepsilon_{\tau R}$$

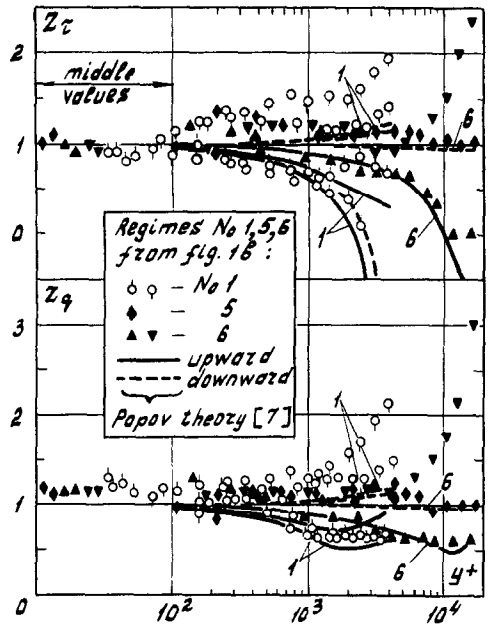

FIG. 6. Relative eddy diffusivity of momentum and heat in the initial stage of the effect of buoyancy.

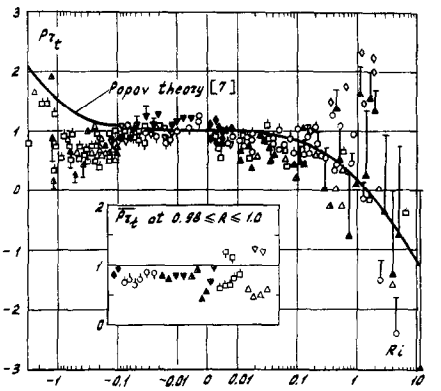

FIG. 8. Turbulent Prandtl number vs Richardson number.

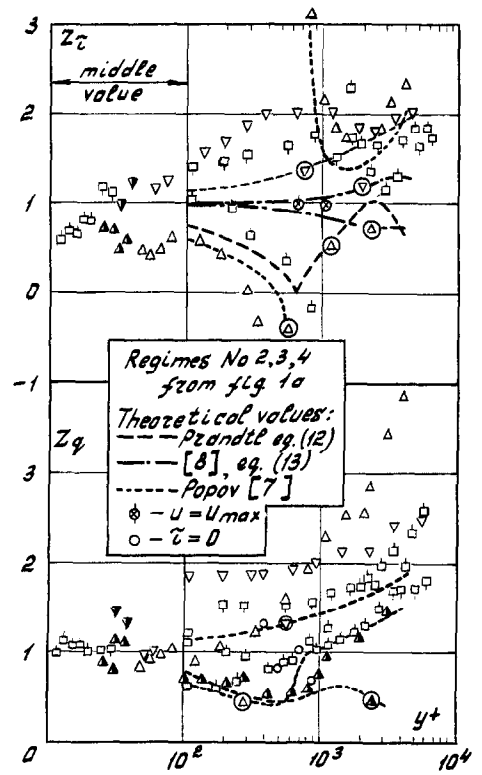

FIG. 7. Relative eddy diffusivity of momentum and heat with substantial effect of buoyancy.

where $\bar{Z}_\tau$ and $\bar{Z}_q$ are constants the values of which were selected from the condition of the agreement on the average between the predicted and experimental values of u and h at $R = 0.97$–0.99. The ratio $\bar{Z}_\tau/\bar{Z}_q$ gives the average value of the turbulent Prandtl number near the wall. The mean data given in Figs. 6–8 correspond strictly to the friction law (3); the correction of the local values was made in those cases when the difference of experimental values of ξ from equation (3) lay outside the limits indicated in Section 2. It should be also noted that the heat transfer data are given for section $x/d \geqslant 32.5$ where a suitable accuracy in the determination of the τ/τ_w and q/q_w profiles is ensured in the approach which was used for processing experimental data. In regimes Nos. 2–4 (upward flow) with $x/d \geqslant 32.5$, there already exists an M-like velocity profile.

In regimes Nos. 1, 5, and 6 (Fig. 1(b)) in which the effect of buoyancy and acceleration are of no consequence (these data are presented in Figs. 6 and 8), the values of ε_τ and ε_q in the near-wall region at $\xi/\xi_N = 1$ correspond well to the transfer model, equation (11), at $Pr_t \approx 0.8 \pm 0.1$. When $\xi/\xi_N = 1.1$, the coefficients $\bar{Z}_\tau$ grow, whereas $\bar{Z}_q$'s drop, and the number $\overline{Pr}_t$ increases up to the level 0.9–1.1, also remaining close to the values which are used for calculating turbulent heat transfer under usual conditions. Conversely, when $\xi/\xi_N = 0.9$, the values of $\overline{Pr}_t$ drop to the level 0.5–0.7 and perceptibly differ from one another in different regimes. This allows a conclusion that at the initial stage of the effect of buoyancy and acceleration the turbulent transfer near the wall is described by the Reichardt model, equation (11), whereas the friction drag in the considered region of thermodynamic states of the fluid satisfies relation (3) with a certain tendency for growing within $\sim 10\%$.

In regimes Nos. 2–4, i.e. in the case of a substantial effect of buoyancy, the coefficients $\bar{Z}_q$ in the near-wall region remain on the average at the level of unity, but the relative coefficients of momentum transfer $\bar{Z}_\tau$ for a downward flow are higher than unity and for an upward flow are much lower than unity, with these differences increasing still greater if it is assumed that

for an upward flow $\xi < \xi_N$ and for a downward flow, vice versa, $\xi > \xi_N$. Accordingly, the values of $\overline{Pr}_t$ in Fig. 8 also scatter.

In all the cases, except for a fully 'normal' regime No. 5, deviations in the transport coefficients from relation (11) are observed in the flow core. They explain the aforegoing features of the flow structure and heat transfer. Thus, already in the initial stage of the effect of buoyancy, Fig. 6 shows clearly the differences in heat transfer in upward and downward flows which are responsible for distinct differences in heat transfer in Fig. 1. With an upward flow the values of $\bar{Z}_\tau$ and Z_q in the flow core are much smaller than unity, with the region of the lowest values coinciding with the flat stretches of the velocity profiles over which the shear stresses are also very small (see Figs. 2 and 5). An appreciable quantitative disturbance of the analogy between the momentum and heat transfer can be noted. In the case of a downward flow, attention is drawn to a strong growth of turbulent transfer in the central portion of the flow. Both phenomena are correlated with a substantial increase in the absolute values of the gradient Richardson number Ri testifying to an increasing role of density fluctuations in the processes of turbulent transfer.

The data of Fig. 7 show that the transition to M-like velocity profiles for the processes considered is of fundamental importance as regards the elimination of tendencies toward heat transfer deterioration. In all the cases, including the sections with minimum heat transfer (the section $x/d = 32.5$ in regimes Nos. 2 and 4), the coefficients Z_q (and Z_τ) $\geqslant 1$ in the trough of the M-like profile and may become even higher than for a downward flow. A certain decrease in heat transport is preserved only over the near-wall stretch of the velocity profile near the surface $\tau = 0$. Note that in all of the cross sections located after the inlet wall temperature peak, the velocity maximum is located much farther from the wall than the surface of zero shear stresses, i.e. there is the region with $Z_\tau < 0$ and the 2nd kind discontinuity ($Z_\tau \to \pm\infty$) testifying to the arbitrariness of the eddy diffusivity ε_τ obtained from equation (1) in the cases considered. With appreciable buoyancy effects the consideration of turbulent heat transfer from the usual standpoints of the hydrodynamic analogy is impossible, since the hydrodynamics itself becomes a function of the heat transfer process. In particular, while the Prandtl–Nikuradze formula [26]

$$\varepsilon_\tau = l^2|\partial u/\partial y| \tag{12}$$

provides an idea about the ranges of variation of the coefficient Z_τ shown in Figs. 6 and 7, the calculation of the values of ε_q from equation (12) at $Pr_t = \text{const.} \approx 1$ would have led to a reduction in heat transfer rate and a distortion of the real pattern of wall temperature variation.

As mentioned above, refs. [6, 7] have suggested techniques for taking into account the effect of buoyancy and acceleration on turbulent transport, including the near-critical region. It is of interest to compare them with the data obtained.

Petukhov and Medvetskaya [6, 8] used the gradient relations (1) for τ and q and determined ε_q in terms of ε_τ and turbulent Prandtl number. Expressions for ε_τ and Pr_t were obtained on the basis of simplified turbulence energy balance equations and intensity of enthalpy fluctuations written down with regard for density fluctuations [27]. After some transformations, the final relation for the eddy diffusivity of momentum can be stated as

$$Z_\tau = \left\{1 + \frac{\chi_1}{Pr_t}\frac{G\beta}{c_p}\frac{\partial h/\partial r}{(\varepsilon_{\tau R}/l^2)^2}\right\}^{1/2} = \left\{1 - \frac{\chi_1}{Pr_t}Ri_L\right\}^{1/2} \tag{13}$$

where Ri_L is the Richardson number to be employed in the case of an undisturbed velocity profile (the Reichardt profile). The coefficient χ_1, selected from experimental data, is a strong function of Re and Y, however, when $Re > 2\times10^5$, i.e. in our case, $\chi_1 = \text{const.} = 1.6$. It is also possible to neglect the change in Pr_t in comparison with the usual value of the order of unity. For the regimes of Fig. 6, relation (13) gives the values $Z_\tau = Z_q \cong 1$. The curves given by relation (13) and constructed for the data of Fig. 7 allow one to conclude that the model considered corresponds qualitatively to the behaviour of the transport coefficients in a downward flow. However, with an upward flow, both the level and the distribution of eddy diffusivities according to relation (13) contradict the experimental data.

On the basis of algebraic relations for turbulent stresses and streams which were obtained by Gibson and Launder [28] and which take into account the contribution of body forces, Popov [7] has come to the following expressions

$$q_t = -\rho\varepsilon_q\,\partial h/\partial y;$$

$$\tau_t = \rho\varepsilon\,\partial u/\partial y - \frac{G\beta}{c_p}\frac{\rho l^2}{Pr_{t0}}\frac{\partial h}{\partial y} = \rho\varepsilon_\tau\frac{\partial u}{\partial y};$$

$$\varepsilon = Pr_{t0}\varepsilon_q = \{\varepsilon_0^2 + \varepsilon_\infty^4/\varepsilon^2 \pm \gamma_1\varepsilon_0\varepsilon_\infty^2/\varepsilon\}^{1/2} \tag{14}$$

where the minus sign refers to $Ri > 0$ and the plus sign to $Ri < 0$;

$$\varepsilon_0 = l^2|\partial u/\partial y|; \quad \varepsilon_\infty = l^2\left(\gamma_2\frac{\beta}{c_p Pr_{t0}}\left|G\frac{\partial h}{\partial y}\right|\right)^{1/2} \tag{15}$$

are the limiting expressions corresponding to the extreme cases $Ri \to 0$ and $Ri \to \infty$. For the constants the following values have been obtained: $\gamma_1 = 1.14$ and $\gamma_2 = 2.24$.

In calculations by this model it was assumed that $Pr_{t0} = 0.9$–1. For determining the mixing path length l, use was made of the hypothesis concerning the conservative nature of the relation $l = l(\tau_w, y, r_0, \rho, \mu)$. At moderate Richardson numbers, $Ri < 1.5$ (it is at almost these values that $\tau_t \approx \tau = 0$ according to equa-

tion (14)) and with $y^+ > 50$ the Popov theory leads to the relationships

$$Z_\tau = C_1\sqrt{\left(\frac{\tau/\tau_w}{R}\right)}; \quad Z_q = \frac{C_2}{Pr_{t0}}\sqrt{\left(\frac{\tau/\tau_w}{R}\right)}, \quad (16)$$

where C_1 or $C_2 = C_1 Pr_{t0}/Pr_t$ are the Richardson number functions which tend to unity when $Ri \to 0$. In this case, the difference of the transport coefficients from the Reichardt model, equation (11), is determined by the relative change in the profile of shear stress as compared with the normal distribution $\tau/\tau_w = R$. The data of Figs. 6–8 show that the Popov theory also describes the quantitative values much better, as well as the behaviour of the experimental values of eddy diffusivities, especially in the region subjected to the effect of the wall, where, strictly speaking, this theory is valid. Systematic discrepancies can be noted in two cases: firstly, in the case of an upward flow in the initial stages of the deformation of the u and τ profiles, when shear stresses in the flow core have not reached zero values as yet but the velocity profile is already very flat and the Richardson numbers are very high so that the theory predicts a considerable decrease in the turbulent Prandtl number, an inverse picture is first observed: $Pr_t \geqslant 1$. To confirm this conclusion, the corresponding points from the regimes with great flow rates of CO_2 are given additionally in Fig. 8 (light rhombs). Secondly, the discrepancy between the theory and test data, just as in the levels of the values of Z_τ, Z_q, so in the numbers Pr_t, is observed in the trough of the M-like profile. Here, when $Ri < 0$, low values of Pr_t are observed in all of the cases, on the average, of the order of 0.6. This testifies to a qualitative change in the mechanism of turbulence in this flow region. High values of transport coefficients and low values of the turbulent Prandtl numbers allow one to speak about a certain analogy with free turbulence. In Fig. 9 the test values of ε_τ for $\partial u/\partial y < 0$ are compared with the Prandtl equation [26]:

$$\varepsilon_\tau = \kappa_1 b(u_{max} - u_{min}), \quad (17)$$

where $b = r_{max}$. It can be noted that in each section

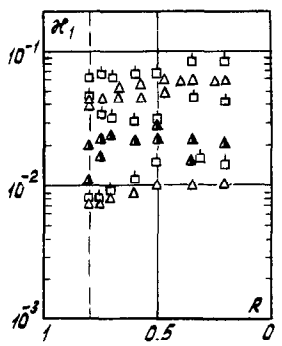

FIG. 9. Free turbulence constant in the trough of M-like velocity profiles.

the constant κ_1 changes slightly along the radius but increases substantially along the tube length. The lowest values of κ_1 are noted in the first instants of the existence of the M-like profile; thereafter they increase and become stabilized. When this circumstance is taken into account numerically, then formula (17) may present one of the versions for solving the problem of the description of turbulent transport in the troughs of the M-like velocity profiles.

The experimental data considered allow one to make one other practical conclusion. Since the inlet wall temperature peaks appear in the initial stages of the transition to the M-like velocity profile, after which heat transfer increases substantially, such a method of the inlet peak equalization may turn out to be effective as the outlining of the heat flux profile in the initial section of the tube which would make it possible to overcome the unpleasant stages of flow deformation at reduced heat loads.

5. CONCLUSIONS

The test data presented allow one to come to the following conclusions:

1. In the case of an upward flow the buoyancy-caused changes in heat transfer take place due to the changes in the structure of the mean flow—in the first place, in the shape of the velocity profile and in the distribution of shear stresses, as a result of which the value and the distribution of the eddy diffusivities of momentum and heat vary. There are no indications of the fact that the change in the turbulent transport could outstrip the change in the averaged flow structure, as is adopted in the theory of the 'initial' effect of buoyancy [27].

The buoyancy-induced deterioration of heat transfer occurs on certain stages of flow rearrangement when the flow develops the regions in which low velocity and shear stress gradients are coupled, i.e. the gradient generation of turbulence energy becomes weaker. In the studied range of high Reynolds numbers ($Re_b > 2 \times 10^5$) such conditions appear in the turbulent flow core and they almost do not affect the viscous and buffer regions of the boundary layer. The development of the M-like velocity profile favour the enhancement of heat transfer in the flow.

Already on the early stages of the effect of buoyancy, there occurs the disturbance of the analogy between the momentum and heat transfer which leads to a substantial difference in the coefficients ε_τ and ε_q. In the case of a substantial effect of buoyancy, the gradient description of momentum transfer, equation (1), in the regions with small velocity gradients and shear stresses is insufficient.

2. In the case of a downward flow, the buoyancy favours the enhancement of turbulent transfer, especially in the flow core, due to which the structure of averaged flow is preserved which is close to the conditions of normal heat transfer. Also preserved is

the stable level of heat transfer but somewhat higher than that predicted from equation (2) in the absence of the buoyancy effect.

The data obtained allow one to speak about the difference between the mechanisms underlying the effect of buoyancy on heat transfer in upward and downward flows.

3. The classical models of turbulent transfer developed for non-perturbed flows do not allow one to adequately describe its variations occurring under the influence of buoyancy. Among the models of turbulent transfer [6, 7] that take into account the effect of buoyancy, the Popov model seems to be more substantiated; in the main features it agrees with the experimental data obtained. The insufficient agreement of the theory [7] with experimental data can be noted in the case of downward flows and also in the region of troughs of the M-like velocity profiles in upward flows.

REFERENCES

1. B. S. Petukhov, Heat transfer in a single-phase medium at near-critical state parameters, *Teplofiz. Vysok. Temp.* **6**(4), 732–745 (1968).
2. W. B. Hall and J. D. Jackson, Heat transfer near critical point, *Proc. of 6th Int. Heat Transfer Conf.*, Toronto, Canada, 1978, Vol. 6, pp. 377–392 (1978).
3. Y. Y. Hsu and J. M. Smith, The effect of density variation on heat transfer in the critical region, *Trans. ASME, J. Heat Transfer* **C83**(2), 176–182 (1961).
4. H. Tanaka, A. Tsuge, M. Hirata and N. Nishiwaki, Effects of buoyancy and of acceleration owing to thermal expansion on forced turbulent convection in vertical circular tubes—criteria of the effects, velocity and temperature profiles, and reverse transition from turbulent to laminar flow, *Int. J. Heat Mass Transfer* **16**, 1267–1288 (1973).
5. E. G. Hauptmann and A. Malhotra, Axial development of unusual velocity profiles due to heat transfer in variable density fluids, *Trans. ASME, J. Heat Transfer* **C102**(1), 71–74 (1980).
6. B. S. Petukhov and N. V. Medvetskaya, Turbulent flow and heat transfer in vertical tubes with strong effect of buoyancy forces, *Teplofiz. Vysok. Temp.* **16**(4), 778–786 (1978).
7. V. N. Popov, Effect of free convection on turbulent transfer in liquid flow through a vertical channel, *Teplofiz. Vysok. Temp.* **21**(3), 515–521 (1983).
8. B. S. Petukhov and N. V. Medvetskaya, Calculation of turbulent flow and heat transfer in heated tubes with single-phase coolants of near-critical parameters, *Teplofiz. Vysok. Temp.* **17**(2), 343–350 (1979).
9. V. N. Popov and Ye. P. Valuyeva, Mixed turbulent fluid convection in vertical tubes, *Teploenergetika* **2**, 17–22 (1988).
10. L. Yu. Krasyakova, I. I. Belyakov and N. F. Fefelova, Hydraulic drag in isothermal and non-isothermal motion of water of post critical pressure, *Teploenergetika* **4**, 31–35 (1973).
11. S. Ishigai, M. Kadji and M. Nakamoto, Heat transfer and pressure drop in a supercritical-pressure water flow, *Trans. Japan Soc. Mech. Engng (JSME), Ser. B* **47**(424), 2333–2349 (1981).
12. R. D. Wood and J. M. Smith, Heat transfer in a critical region—temperature and velocity profiles in turbulent flow, *A.I.Ch.E. Jl* **10**(2), 180–186 (1964).
13. P. J. Bourke and D. J. Pulling, Experimental explanation of deterioration in heat transfer to supercritical carbon dioxide, ASME Paper No. 71-HT-24 (1971).
14. Z. L. Miropolskiy and V. I. Baigulov, Heat transfer velocity and temperature distribution in carbon dioxide tube flow in the near-critical region of parameters, *Heat Transfer—74—Soviet Research*, pp. 81–89. Izd. Nauka, Moscow (1975).
15. B. S. Petukhov, V. A. Kurganov and V. B. Ankudinov, Heat transfer and hydraulic drag in turbulent tube flow of fluid of near-critical state parameters, *Teplofiz. Vysok. Temp.* **21**(1), 92–100 (1983).
16. V. A. Kurganov, V. B. Ankudinov and A. G. Kaptilnyi, Experimental study of velocity and temperature fields in an upward flow of carbon dioxide of supercritical pressure in a vertical heated tube, *Teplofiz. Vysok. Temp.* **24**(6), 1104–1111 (1986).
17. V. A. Kurganov, V. B. Ankudinov and A. G. Kaptilnyi, Hydraulic drag and heat transfer in vertical heated tubes at supercritical pressures of heat carriers. The structure of turbulent supercritical pressure carbon dioxide flow in a vertical heated tube. In *Turbulent Mixed Convection Heat Transfer in Vertical Tubes*, pp. 95–201. Izd. IVTAN, Moscow (1989).
18. M. J. Watts and C. T. Chou, Mixed convection heat transfer to supercritical pressure water. In *Heat Transfer—82*, Vol. 3, pp. 495–500. München (1982).
19. V. A. Kurganov and V. B. Ankudinov, Calculation of normal and deteriorated heat transfer in tubes in turbulent fluid flow in the near-critical and gas regions of state, *Teploenergetika* **6**, 53–57 (1985).
20. D. A. Labuntsov, Some problems of convective heat transfer in the supercritical region, *Teploenergetika* **3**, 69–72 (1972).
21. V. A. Kurganov, A. G. Kaptilnyi and V. B. Ankudinov, Hydraulic drag and friction resistance in upward and downward supercritical pressure fluid flow in heated tubes, *Teplofiz. Vysok. Temp.* **27**(1), 94–103 (1989).
22. B. S. Petukhov and V. N. Popov, Theoretical calculation of heat transfer and friction in turbulent tube flows of incompressible fluid with variable physical properties, *Teplofiz. Vysok. Temp.* **1**(1), 85–101 (1963).
23. P. L. Maksin, B. S. Petukhov and A. F. Polyakov, Calculation of turbulent momentum and heat transfer in incompressible liquid and gas tube flow with variable physical properties. In *Problems of Convective and Radiative-Conductive Heat Transfer*, pp. 5–42. Izd. Nauka, Moscow (1980).
24. V. A. Kurganov and N. V. Medvetskakya, Influence of supercritical fluid parameters on turbulent flow characteristics, *Proc. Int. Seminar on Near-Wall Turbulence*. Dubrovnik, Yugoslavia (1988).
25. H. Reichardt, Die Grundlagen des turbulenten Wärmeübergangs, *Arch. Ges. Wärmetechnik* **6/7**, 129–142 (1951).
26. H. Schlichting, *Grenzschicht-Theorie*. G. Braun, Karlsruhe (1965).
27. B. S. Petukhov and A. F. Polyakov, *Mixed Turbulent Convection Heat Transfer*. Izd. Nauka, Moscow (1986).
28. M. M. Gibson and B. E. Launder, On the calculation of horizontal, turbulent, free shear flow under gravitational influence, *Trans. ASME, J. Heat Transfer* **C98**(1), 81–89 (1976).